Composites

Dielectrics of graphene oxide decorated with nanocomposite silica-coated calcium copper titanate (CCTO) nanoparticles

Debasrita Bharatiya[2] , Santhosh Kumar[2] , S. Raghunandan[3] , and Pradip Paik[1,2,*]

[1] School of Biomedical Engineering, Indian Institute of Technology (IIT)-BHU, Varanasi, Varanasi, UP 221005, India
[2] School of Engineering Sciences and Technology, University of Hyderabad, Hyderabad, Telangana 500046, India
[3] Center for Nanotechnology, BHEL Corporate R & D, Vikas Nagar, Hyderabad, Telangana 500093, India

ABSTRACT

This work presents the synthesis of the noble nanocomposites of silica-coated calcium copper titanate–graphene ($CCTO@SiO_2$–GO) by the established sol–gel method. This paper showed the decoration of $CCTO@SiO_2$ NPs on the surface of graphene oxide and how the decoration/attachment depends on various environmental and instrumental factors like sonication time, stirring rate, centrifugation rpm and the thickness of silica shell coated on CCTO NPs. The prepared $CCTO@SiO_2$–GO composites were characterized by suitable characterization techniques. FESEM and TEM confirmed the morphological study of nanocomposites and how the $CCTO@SiO_2$ NPs are attached to the surface of GO sheet. FTIR has shown the presence of O–H, N–C groups which help in the formation of types of bonds between $CCTO@SiO_2$ NPs and GO. This work further revealed an excellent result of a dielectric study, indicating that the best-decorated $CCTO@SiO_2$ NPs over the surface of the GO sheet cause the increment of dielectric constant ε' from 10^2 up to 10^5. Meanwhile, this study also suggested high loss ε'' up to 10^6 at a lower frequency, i.e. 20 Hz at RT which can be useful for microelectronic devices. This variance of dielectrics is due to the effect of polarization and decoration of $CCTO@SiO_2$ NPs over the GO sheets. As the frequency increases from 20 Hz to 2 MHz, the dielectric constant ε', as well as the loss of ε'', reached up to 10^2 values for the highest decorated material. Our study also clearly explained a uniform variation in dielectric constant ranges from 1×10^2 to 1.5×10^4 at a different temperature range from room temperature to 560 °C with a frequency range of 3×10^4 Hz to 2×10^6 Hz, and the value varies accordingly with the synthesis method.

Address correspondence to E-mail: paik.bme@iitbhu.ac.in

Introduction

Earlier studies have provided the information of graphene oxide (GO) as a two-dimensional (2D) material, a flat monolayer of sp^2 hybridized carbon atoms, tightly packed into a honeycomb lattice and a basic synthetic frame for all graphene materials [1, 2]. Recent studies of graphene oxide have been attracting many researchers towards itself due to its significant advantages of electrical stability, highly stable thermal and mechanical properties along with biocompatible nature [3–5]. Contemporary research has also shown the applications of graphene oxide (GO) in the development of 3D smart material, pressure-based biosensors and nanohybrid materials [6–8]. Reports are available for the impermeable membranes which are associated with GO, leading to the creation of pressure differences between itself and atmosphere, becoming an advantage for the microfabrication of devices by calculating its mass and elastic constants [9]. The structural distortion feature along with the presence of various oxygen moieties on the mono-/multilayers of GO has proved its excellence towards the applications in biology, chemistry and engineering field [10–12]. As reported earlier, GO has shown a high dielectric constant (ε') of 10^6 with low loss (ε'') of 10^2, becoming useful in electronic and optical devices, thin films, sensors, etc. [13]. Fundamental dielectric study has established the calcium copper titanate (CCTO, $CaCu_3Ti_4O_{12}$) as the best dielectric material, which possesses a high dielectric constant of $\sim 10^5$ and a low loss due to its perovskite nature of having a wide area of applications in charge storage devices, sensors, etc. as compared to other ferroelectric materials (ε' 1×10^3–5×10^4) [14–16]. However, as an exception to the ferroelectric material, temperature-independent behaviour of CCTO from RT to 500 K, with a giant constant and a very low, loss showed an exceptional result to the dielectric study which encourages us to go for further development of new nanocomposites including CCTO nanoparticles (NPs) and GO sheets [17–19]. GO and silica-coated calcium copper titanate (CCTO@SiO$_2$) NPs were synthesized from the established Hummer's method and sol–gel process, respectively [20, 21]. From the literature, it is clear that the increase in shell thickness of CCTO NPs leads to the gradual decrease in dielectric constant ε' and loss ε''. In contrast to the silica thickness over dielectric constant, our work has revealed an interesting fact that the effect of silica shell thickness could not cease the real part of dielectrics ε', whereas the effect of spreading of core–shell NPs on the GO sheet becomes prominent. The effect of the decoration of CCTO@SiO$_2$ NPs with the best positioning causes the nanocomposite material to increase the dielectric constant ε' and loss ε'' within the frequency range of 20 Hz–2 MHz. The study of temperature-dependent dielectrics with respect to variable frequency showed exceptional behaviour towards the effect of spreading which is not clear in this case. This might be either due to the charge polarization effect with a change in dipole moment. Various characterization techniques help in the analysis of synthesized silica-coated calcium copper titanate on graphene oxide (CCTO@SiO$_2$–GO) nanocomposite to confirm its several chemical properties and physical behaviour. The dielectric study of these nanocomposites reveals a very different and significant study of the decorated CCTO@SiO$_2$–GO nanocomposites.

Experimental section

Materials and method

Graphite powder (synthetic powder, Sigma-Aldrich), sulphuric acid (conc. H_2SO_4, 95.0–98.0%, ACS reagent, Sigma-Aldrich), potassium persulphate ($K_2S_2O_8$, > 99%, ACS reagent, Sigma-Aldrich), phosphorous pentoxide (P_2O_5, 99.9%, Sigma-Aldrich), potassium permanganate ($KMnO_4$, 99.9%, Sigma-Aldrich), hydrogen peroxide (H_2O_2, Sigma-Aldrich), hydrochloric acid (dil. HCl solution, 37%, ACS reagent, Sigma-Aldrich), calcium carbonate (anhydrous $CaCO_3$, 99.9%, Sigma-Aldrich), titanium dioxide (powder TiO_2, 99%, Sigma-Aldrich), cupric oxide (powder CuO, 99%, Sigma-Aldrich), tetraethylorthosilicate (TEOS, 98%, reagent grade, Sigma-Aldrich), (3-aminopropyl) triethoxysilane (APTES, > 98%, Sigma-Aldrich), ammonium hydroxide (NH_4OH, 95%, Sigma-Aldrich) and IGEPAL (viscous liquid, Sigma-Aldrich) were used for further modification. Cyclohexane (C_6H_{12}, 99.5%) and ethanol (C_2H_5OH, < 99.9% pure) were purchased from Finar chemicals.

Synthesis of GO

Graphene oxide (GO) was synthesized from an established Hummer's method. We have reported the synthetic procedure for GO in our previous work [22].

Synthesis of CCTO@SiO$_2$ NPs

CCTO@SiO$_2$ NPs were synthesized by the general sol–gel method and cyclohexane as an appropriate solvent. CCTO@SiO$_2$ NPs have been successfully synthesized by following the sol–gel synthetic method. 1 gm of CCTO NPs was taken with 130 ml of cyclohexane and allowed under ultrasonication for few minutes. 5 ml of IGEPAL-50 was added dropwise to the given solution and allowed under ultrasonication for 30 min. The ratio of IGEPAL-50 to conc. NH$_4$OH was maintained with the previously used condition and added to the above solution dropwise. The solution mixture was allowed under sonication for 30 min. Various ratios of silica (APTS: TEOS) have been used for the synthesis of CCTO@SiO$_2$ NPs through sonication and centrifugation process maintaining other environmental parameters too. After 48 h of reaction on a shaker at 600 rpm, the products were collected by centrifugation and were washed with distilled water followed by ethanol.

Synthesis of CCTO@SiO$_2$–GO

CCTO@SiO$_2$–GO nanocomposites were synthesized using the modified sol–gel method, in which CCTO@SiO$_2$ NPs and GO act as precursor materials which are previously synthesized by Hummer's method and sol–gel process, respectively. The mixture is allowed under hydrolysis process and sonication for few minutes in different ratios. These solutions are poured into a reagent bottle and allowed for sonication for 4 h by consistently maintaining at room temperature (RT). Several decoration types of CCTO@SiO$_2$–GO nanocomposites mainly

depended on few environmental parameters given in Table 1. The concept of covalent bonding of silica and GO or amide bonds may play a role in the synthesis of CCTO@SiO$_2$ NPs on the surface GO sheet. The reason for choosing water as a suitable solvent in synthesis is mainly due to the solubility of product composites. FTIR study has shown a clear image of C–N bond present in the composites which may arise due to the interaction between carboxylic –COOH, hydroxyl (–OH) or ether (–O–) of GO and –NH$_2$ or SiO$_2$ groups of CCTO@SiO$_2$ NPs. C–N bond is strongly polarized towards N due to the presence of lone pair in N, so the dipole moment arises, making C–N bond soluble in water [23]. After the process of sonication is completed, the solution bottle is kept in a shaker for 72 h at 600 rpm. With the completion of 3 days, the composite material was continuously centrifuged with distilled water at high rpm 14000 for 30 min at very low temperature. Once the centrifugation is over, the material was allowed for drying at 100 °C and the grey colour material was collected. Various steps of the sol–gel synthesis method of CCTO@SiO$_2$ NPs are shown in Scheme 1.

We did several experiments, but among all the synthesis procedure, it is confirmed that at higher rpm, the centrifugation process helps in better extraction of water-like solvent along with unnecessary surfactant from the final product of the composite material. This method also signifies that more time of shaking also enhances the spreading/decorating capability of silica-coated CCTO on the surface of GO.

Characterization techniques

The particles were characterized by various techniques, e.g. XRD, FESEM/TEM, FTIR, Raman, TGA, UV and impedance spectrometry, to confirm the crystallinity, morphology, chemical composition, the vibrational or rotational motion of atoms, the thermal stability of the material, absorbance of electronic transition and the variation in dielectric behaviour at

Table 1 Synthesis of CCTO@SiO$_2$–GO nanocomposites at different conditions

Sample name	CCTO@SiO$_2$ NPs	Amount of CCTO@SiO$_2$ NPs	Amount of GO NPs	Shell thickness	Sonication time	rpm
CSG1	CS3	50	50	3 nm	45 min	14000
CSG2	CS7	50	50	5–7 nm	3 h	14000
CSG3	CS16	100	25	15–20 nm	3 h	12000

Scheme 1 Schematic steps of the sol–gel synthesis method of CCTO@SiO$_2$ NPs.
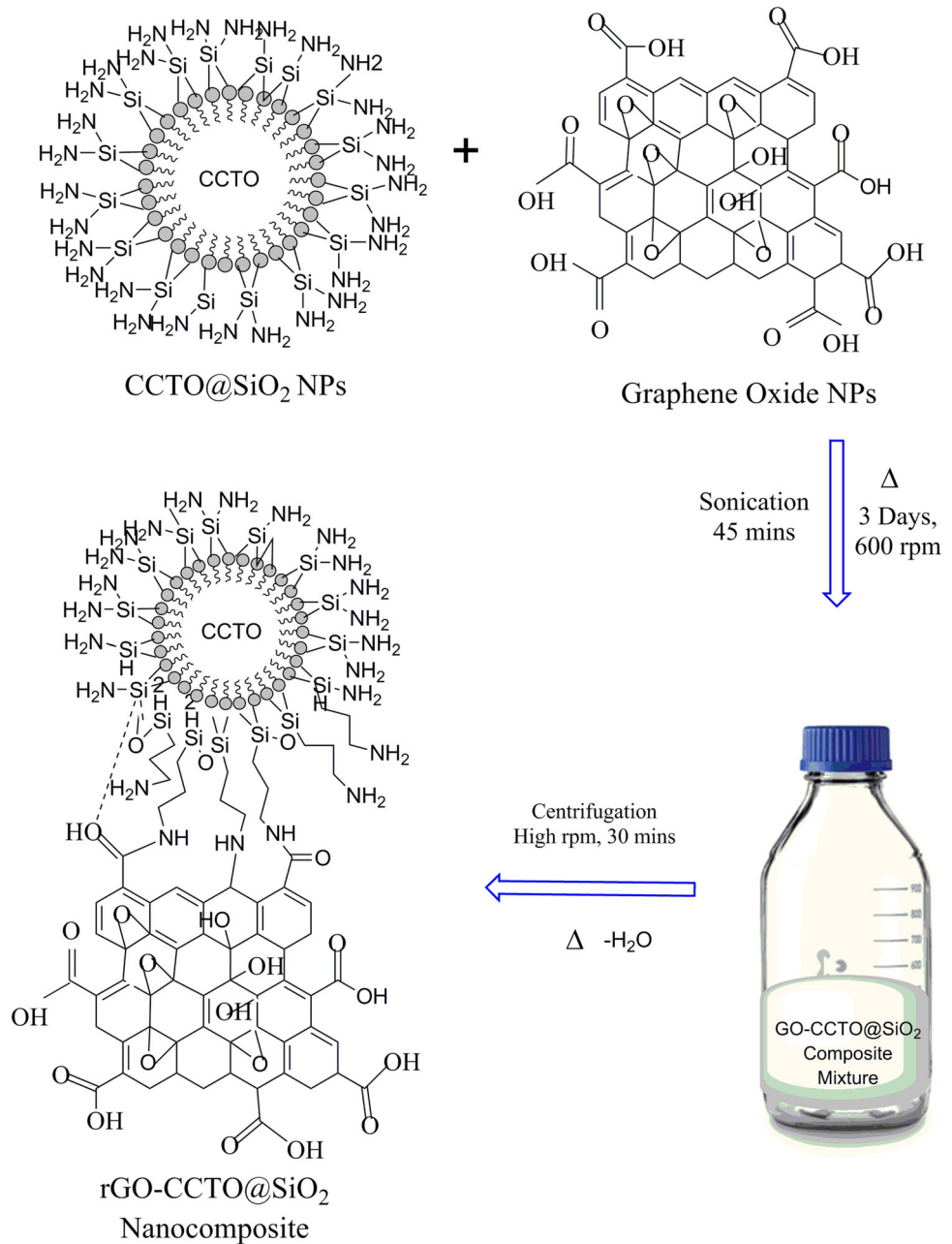
different frequencies and temperatures, respectively. Characterizations of the grey-coloured powder samples of CCTO@SiO$_2$–GO nanocomposites were done by involved scientific instruments. Distinguished crystalline and amorphous nature of the samples of silica, CCTO and GO was studied by using X-ray diffraction (XRD) technique. The XRD experiments were carried out on Bruker AXS Model D8 Advance X-ray diffractometer. Elemental detection was done by FESEM. The FESEM experiments were done by Hitachi S-3400 N. Morphological studies and diffraction pattern and fringe studies were also carried out using a transmission electron microscope (TEM) (model FEI Technai G2 S–Twin). Raman scattering study was carried out using WITech alpha 300 Raman spectrometer for the study of vibrational as well as rotational motions of atoms and molecules present in the CCTO@SiO$_2$–GO nanocomposites. The thermal study including the weight loss percentage, amount of heat flow and phase transition was done by TG/DTA (Thermo ONIX Gaslab 300). The TG/DTA study was done in inert N$_2$ atmosphere from 30

to 1000 °C at a heating rate of 10 °C. The study of chemical composition and the presence of organic functional groups of the sample were studied by FTIR (Nicolet model impact—410). For the study of FTIR analysis, CCTO silica composite was mixed with KBr by grinding in an agate mortar followed by making pellets. FTIR spectrum was obtained after removing unnecessary background format. UV–Vis NIR experiment was done in LAMDA 750 spectrometer (PerkinElmer). The dielectric study of material CCTO@SiO$_2$–GO nanocomposites was done by impedance spectrometer after preparing the pellets. The pellets were prepared by general method, i.e. adding PVA as binder and water to help the powder mixed properly to give a better result. The pellet preparation method is the same as available in our previous work [22].

Results and discussion

Figure 1a shows that the HRTEM image suggests that uncoated pure CCTO has been successfully synthesized with diameter range 200 nm and length 500 nm. Figure 1b shows that the HRTEM micrograph has confirmed the formation of silica-coated CCTO (CCTO@SiO$_2$) NPs, bearing silica shell thickness of 2–3 nm. GO sheet is shown clearly in Fig. 1c with the transparent pattern and layers which is alike reported earlier and further confirmed by FESEM images of Fig S1(a) and S1(b). The layer shapes of Fig S1(c) and fig S1(d) are modified to folded like sheet, due to the interaction of the functional groups present in the GO sheets and experimental factors. From these images, it is also noticed that a number of random unshaped particles are attached to the layer of GO which may indicate the presence of CCTO@SiO$_2$ core–shell particles. HRTEM images in Fig. 1d (low magnification) and Fig. 1e (high magnification) clearly confirm the attachment/decoration of 2–3-nm-thick silica-coated CCTO (CCTO@SiO$_2$) core–shell NPs over GO surface. This could be possible only by the formation of enormous covalent bonding between GO and CCTO@SiO$_2$ NPs which further have been confirmed through FTIR results. There are various possibilities of bonding which may include hydrogen molecular bonding due to the presence of secondary amine group of CCTO@SiO$_2$ core–shell NPs, –COOH groups of GO, C–N covalent bond attached to the Si–O–GO surface [10].

Composites were synthesized in the water medium to facilitate the formation of C–N bonds between –COOH, –OH or –O– of GO and –NH$_2$ or SiO$_2$ groups of CCTO@SiO$_2$ NPs. C–N bond is strongly polarized towards N due to the presence of lone pairs in N so the dipole moment arises, making C–N bond soluble in water [23].

From fig S1(e) and Table S1(f), the EDS spectra of CCTO@SiO$_2$–GO-2 (CSG2) confirmed that all the precursor materials, i.e. SiO$_2$, CCTO, CCTO@SiO$_2$ including Cu, Ti, O, C and Si, are present. GO property helps itself to undergo the formation of sheets which enhances the surface area of GO, so its weight percentage is more compared to Cu, Ti and Si, whereas we have taken the same amount of CCTO@SiO$_2$ and GO (1:1) [24]. The dark colour particles represent Si-coated CCTO, and the brighter parts represent for the GO sheet NPs. Here a number of particles attached to the surface are seen to be less and not effectively coated all over the surface of the GO sheet. In the later study, we will discuss the better coating of CCTO@SiO$_2$ NPs on the GO sheet. Figure 1e gives a better idea of how CCTO@SiO$_2$ NPs are attached to the GO sheet. Figure 1e, g, i clearly shows that the transparent nature of GO for single or few layers is due to the GO impermeable property [25]. Figure S2(a) shows an effective coating of CCTO@SiO$_2$ on GO sheet as the dark-coloured material is well spread over the brighter material, so in other images it shows the brighter particles clearly but not in this image. It is a well-occupied material and may be due to the effect of stirring time which helps CCTO@SiO$_2$ to adsorb all over the GO sheet. The concept of adsorption signifies the morphology of CCTO@SiO$_2$–GO composites that CCTO@SiO$_2$ molecule acts as an adsorbate on the surface of GO sheet as an adsorbent. Figure 1f shows a near view of fig S2(a) which helps us to see the particles very clearly. Figure 1h and fig S2(b) represent the 15–20-nm silica-coated (CCTO@SiO$_2$) NPs that are attached to the surface, and it is shown that the excess of silica whatever attached to CCTO NPs has come out from the core–shell and formed agglomerations in few places. It may be due to the effect of excess sonication time or else increased rpm of the centrifugation process. Figure 1j–l illustrates the IFTT images with a d-spacing value of 0.525 nm, 0.419 nm and 0.398 nm for pure CCTO NPs, CCTO@SiO$_2$ NPs and CCTO@SiO$_2$ NPs over GO, respectively.
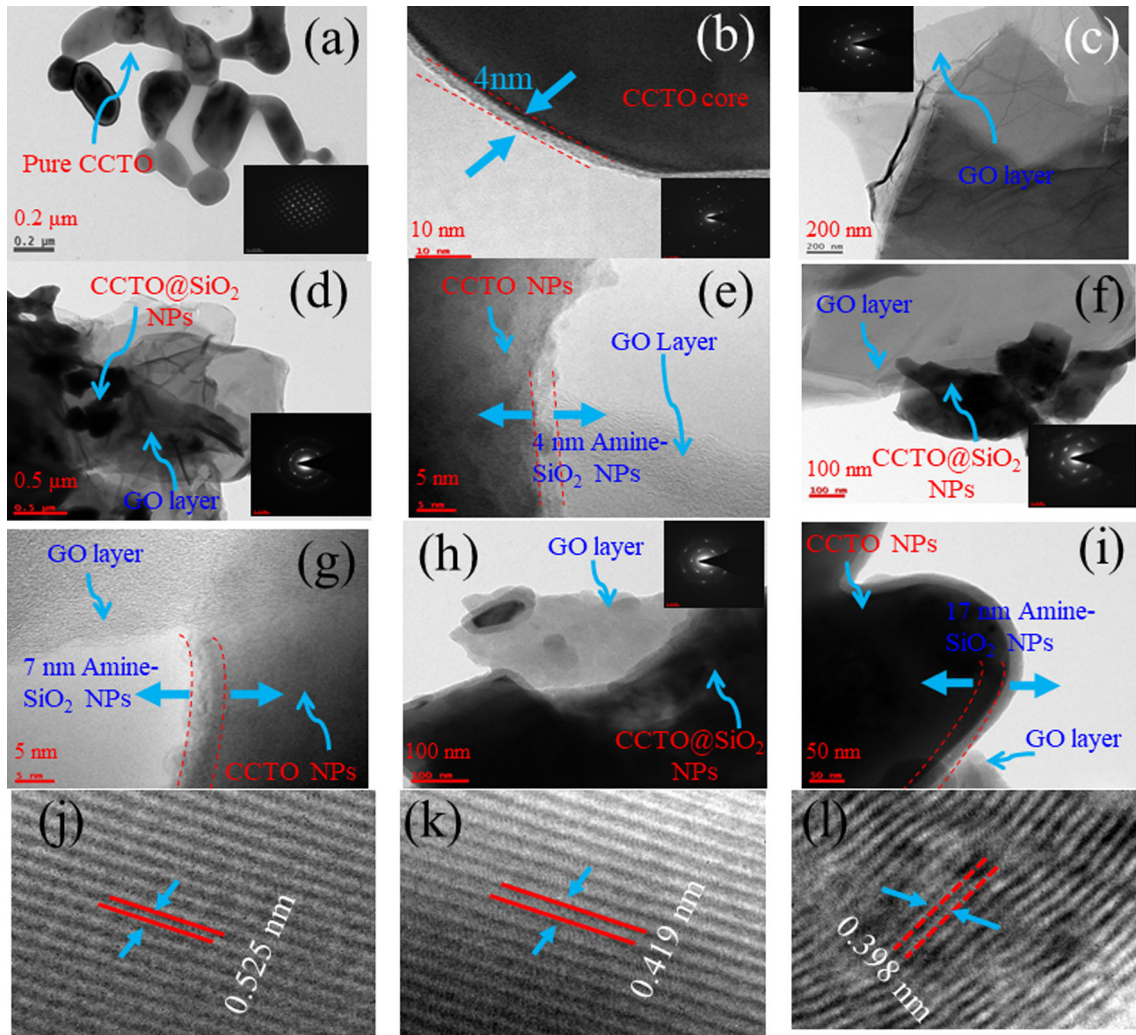
Figure 1 a–c HRTEM images of pure CCTO NPs, coated CCTO@SiO₂ NPs and GO, respectively. **d**, **f** and **h** Coating of CCTO@SiO₂–GO NPs named as CSG1, CSG2 and CSG3, respectively. **e**, **g** and **i** Shell thickness of silica-coated on CCTO NPs which are attached on the surface of GO layers of thickness 2–4 nm, 5–7 nm and 15–17 nm, respectively. **j–l** IFTT images with d-spacing values of pure CCTO NPs, CCTO@SiO₂ core–shell NPs and CCTO@SiO₂ NPs over GO, respectively.

The crystalline structure of the nanocomposite was confirmed by XRD. GO shows its peak in the range of 7–10 2θ with Cu Kα radiation [26]. Inset in Fig. 2a shows very similar peaks for GO, pure CCTO and silica-coated CCTO NPs [20, 22]. But after the reduced synthesis of CCTO@SiO₂–GO nanocomposites, GO is showing its peak at 25 with Cu Kα radiation. It may be because GO is reduced with water or with other precursor materials of CCTO@SiO₂ NPs. In HRTEM images we discussed the bonding between CCTO@SiO₂ and GO surface, and here, we conclude that GO converted to r–GO showing the peak range at 25 (2θ) with Cu Kα radiation which confirms the crystallinity of GO NPs or it may

happen that shifting causes may be due to the decrease in spacing between the layers of GO shown in Fig. 1j–l on reduction helps in the broad peak of GO at the peak value of 9 at 2θ shifted towards 25, making it more diffused, i.e. small hump like a peak. Meanwhile, Fig. 2a represents the other two theta values of 30, 35, 38, 43, 46, 49, 63 and 74 like (211), (220), (310), (222), (321), (400), (422) and (440) shows the presence of CCTO patterns [17]. But it is not showing any peaks for silica. It may be due to very less weight percentage of Si present in the material, but the presence of silica is already confirmed from the earlier EDS analysis in fig S1(e).
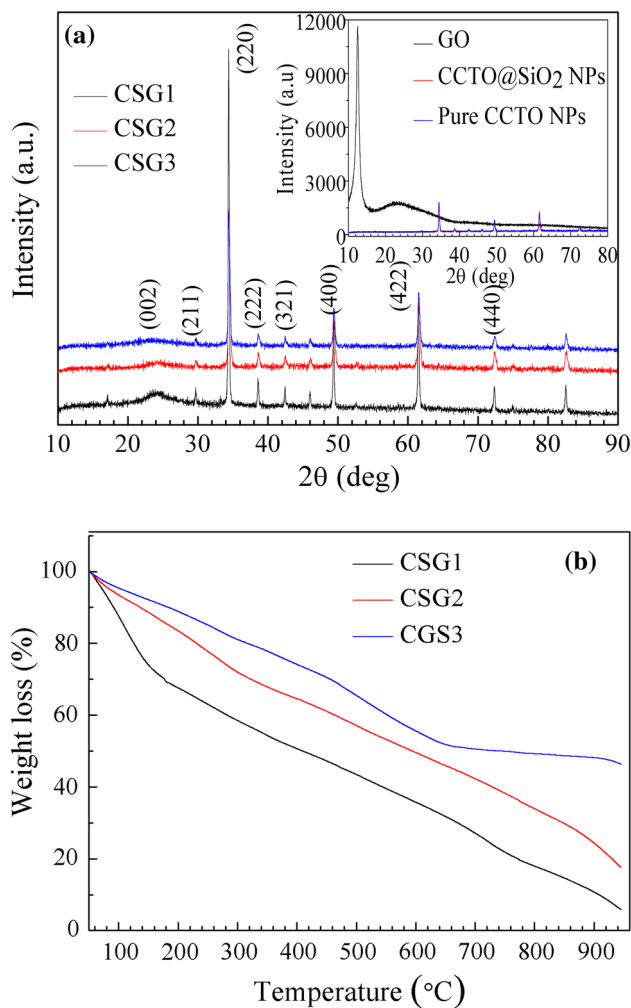
Figure 2 a XRD pattern and b TGA thermogram for CSG1, CSG2 and CSG3 nanocomposites synthesized from 2–4-nm, 5–7-nm and 15–17-nm Si-coated CCTO, respectively.

Figure 2b represents the TGA thermogram of CSG1, CSG2 and CSG3 nanocomposites synthesized from 2–4-nm, 5–7-nm and 15–17-nm Si-coated CCTO NPs, respectively, at inert atmosphere, heating rate 10 °C/min. It is clear that GO shows thermal instability between RT and 1000 °C. The factor of the highest percentage of coating or well spreading of material over the surface shows an exceptional behaviour as compared to another disturbed coating. It is mentioned earlier that a significant weight loss occurs in GO NPs [27]. The total weight loss % of CSG1 and CSG2 is ∼ 80% and 92%, whereas for CSG3 it is only 50%. The less weight loss in CCTO@SiO2 with highest coating thickness is due to the presence of silica which has higher thermal stability. In the former case, weight loss is mainly

between 150 and 250 °C and the loss % is ∼ 25%, and this may be due to the presence of some by-product gases like H_2O, CO_2, etc. CSG1 shows a gradual decrease in weight loss from 250 to 900 °C without any significant changes, and its weight loss finally reaches 80%. But in the case of CSG2, the weight loss has been remarkably occurred in between 300 and 500 °C and the loss % is 92%.

Hence, it is proved that the highest silica-decorated CCTO core–shell NPs on the GO sheet are not thermally stable in nature. In contrast to both CSG1 and CSG2, the highest silica-coated CCTO over GO, i.e. CSG3, is showing lowest 50% of weight loss with maximum stability at high temperature 1000 °C. The sudden weight loss may occur due to the breaking of the covalent bond between the amine group of silica and carboxy (–COOH)/hydroxyl (–OH) group of GO, or other functional groups attached to the silica-coated CCTO have been decomposed between this range.

Figure S3(a) represents FTIR spectra for GO, pure CCTO NPs and CCTO@SiO2 NPs, which resemble peaks like CCTO NPs at 560 cm^{-1}, 590 cm^{-1} and 450 cm^{-1} for Ti–O and Cu–O str, while GO has shown peak near 1643 cm^{-1}, 1095 cm^{-1} and 1198 cm^{-1} for aromatic C=C, C–O alkoxy group and C–O epoxy groups, confirming the precursor for synthesized nanocomposites. Figure 3a suggests the chemical functionality of the decorated CCTO@SiO2–GO composite. In this plot, it is clearly shown that the schematic diagram of CCTO@SiO2–GO composite exists with the group functionality proof. The OH bond of the GO can be observed at 3413 cm^{-1}. The stretching vibration band at 1724 cm^{-1} was associated with the stretching of the free –C=O or –COOH bond which is arisen due to the unreacted carbonyl groups in GO with core–shell NPs. The characteristic peak of the silica can be seen at 1235 cm^{-1} (Si–O–Si, asymmetric stretching). 1570 cm^{-1} peak has been observed and is responsible for the formation of N–C asymmetric stretching mode; it may be arisen due to the bonding interaction of amine group of CCTO@SiO2 NPs and hydroxyl of carboxylic group of GO NPs. The peaks of 563 cm^{-1}, 557 cm^{-1} and 447 cm^{-1} show the presence of precursor materials Ti–O, Cu–O and Ca–O in bending modes, respectively. GO has epoxy groups before the experimental synthesis procedure, but after the required process, the nucleophilic O of the epoxy group may be converted to a hydroxyl group and electrophilic C–H
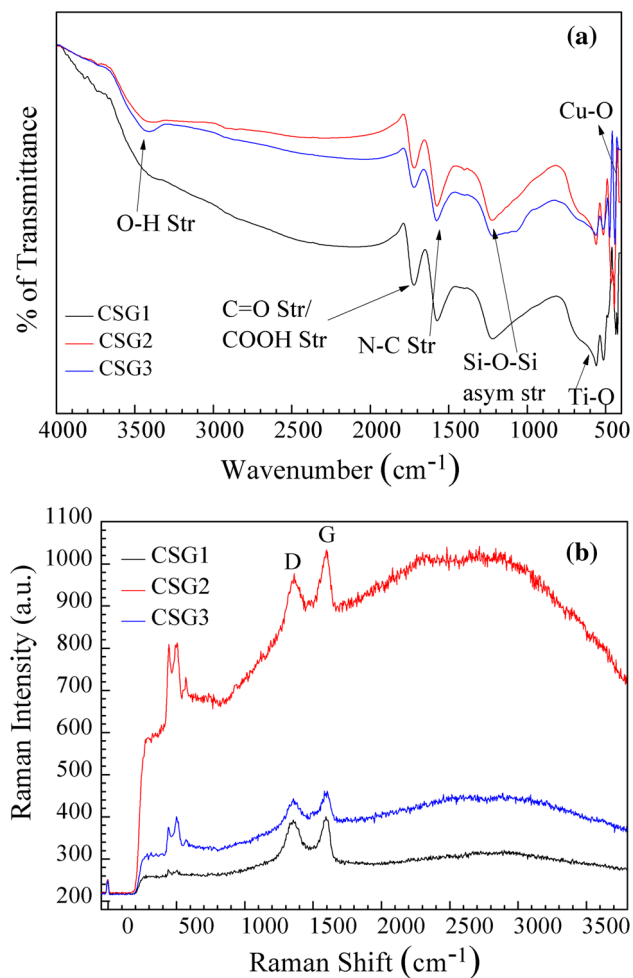
Figure 3 a FTIR spectra and **b** Raman spectra for CSG1, CSG2 and CSG3 nanocomposites synthesized from 2–4-nm, 5–7-nm and 15–17-nm Si-coated CCTO NPs, respectively.

group attached to the nucleophilic part of the Si-coated CCTO NPs [27, 28]. CCTO is a perovskite material [17], and it does not have any organic functional group in the material, so coated silica-bearing functionalized amine group is helping in the fabrication of this nanomaterial composite. CSG2 is showing the highest percentage of transmittance that means maximum frequency passed straight through this material without being absorbed as it is well spread over the surface of GO.

After going through the Raman literature for CCTO, silica-coated CCTO NPs and GO, we have observed a very similar vibrational mode result for the precursors of nanocomposites of CCTO@SiO$_2$–GO. Figure S3(b) confirms the peaks at 1353 cm^{-1} (D band) and 1593 cm^{-1} (G band) for GO, whereas very similar peaks were observed at 444 cm^{-1}, 503 cm^{-1},

572 cm^{-1}, 1122 cm^{-1} and 1324 cm^{-1} for CCTO as well as core–shell CCTO@SiO$_2$ NPs. Figure 3b shows the Raman spectrum of the synthesized nanocomposite as it is a non-invasive method to give a huge information about the randomness of atoms and the thermal conductivity of a nanocomposite material [29]. The CCTO@SiO$_2$–GO composite shows two important bands of Raman spectrum irradiated by an electron laser beam, showing significant and strong D peaks at 1386 cm^{-1}, 1394 cm^{-1} and 1353 cm^{-1} and G peaks at 1586 cm^{-1}, 1602 cm^{-1} and 1602 cm^{-1} for CSG1, CSG2 and CSG3 which is very similar to D band at 1350 cm^{-1} and G band at 1580 cm^{-1} of GO sheet [30]. TEM images of the material suggested the presence of multilayer of the prepared nanocomposite. As the number of graphene oxide layers increases, the shift of spectrum occurs and it mainly depends on the polarization of atoms through various angles [31]. Here G band and D band for GO are at 1602 cm^{-1} and 1394 cm^{-1}, whereas TiO$_6$ rotation and O–Ti–O anti-stretching show their peak at 439 cm^{-1} and 494 cm^{-1} for highest coated CCTO@SiO$_2$–GO-3. Its intensity is very high as compared to other decorated materials that are given in Table 2. The G band is shifted to 1602 maybe due to the presence of isolated organic unsaturated bonds in the material [32–34] which resonate at a higher frequency. Table 2 shows the concept of Raman modes of vibration of synthesized nanocomposites of CCTO@SiO$_2$–GO.

As the disorder randomness increases, Raman intensity increases with separate disorder peaks. It is proved that longitudinal optical phonon mode is active near the armchair edge, whereas transverse optical phonon mode is active near the zigzag edge. So this is because the G band intensity is enhanced from 1580 to 1602 cm^{-1}. Hence, it is concluded that the polarization of the excitation layer is parallel to the armchair edge and perpendicular to the zigzag edge.

Figure 4 clearly shows the UV–visible spectra in which GO is showing the highest intensity peak, whereas other coated CSG1, CSG2 and CSG3 nanocomposites, as well as pure CCTO, show a very less intensity. The effect of coating on GO is not allowing to occur the excitation of electrons from the surface in addition to the absence of high-intensity peaks. This above figure clearly shows the absence π–π interactions of graphene oxide with any of the CCTO@SiO$_2$–GO nanocomposites where Pure GO

Table 2 Raman modes of vibration of newly synthesized nanocomposites of CCTO@SiO₂–GO

Name of the composite	D band (cm^{-1})	G band (cm^{-1})	D band (intensity)	G band (intensity)
CSG1	1386	1586	371	391
CSG2	1394	1602	953	1033
CSG3	1353	1602	443	461
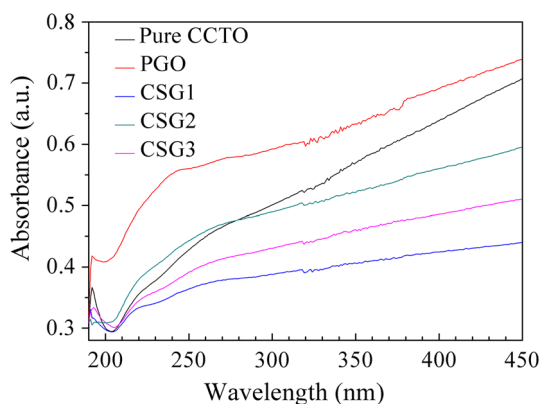
Figure 4 UV–Vis NIR spectra of pure CCTO NPs, GO NPs, CSG1, CSG2 and CSG3 nanocomposites synthesized from 2–4-nm, 5–7-nm and 15–17-nm Si-coated CCTO, respectively.

(PGO) is showing a clear excitation near 570 nm [35, 36].

Study on frequency- and temperature-dependent dielectrics of CCTO@SiO₂–GO nanocomposite

Dielectric behaviour with respect to change in frequency

Figure 5a represents the plot for the variation in dielectric constant, with respect to frequency range from 1×10^3 Hz to 1×10^6 Hz for of CSG1, CSG2 and CSG3 nanocomposites synthesized from 2–4-nm, 5–7-nm and 15–17-nm Si-coated CCTO core–shell NPs, respectively. Although the experiment was started at 20 Hz as lowest frequency, due to an instrumental error we have avoided the data from 20 Hz and have shown from 1×10^3 to 2×10^6 Hz. Complete data including dielectric along with impedance constant are given in Table S1 and Table S2. Figure 5a, b clearly shows about CSG2 which is showing a highest dielectric constant ε' of $\sim 3 \times 10^5$ and loss of $\varepsilon'' \sim 1 \times 10^6$ at 1×10^3 due to the highest decoration property. The HRTEM image of Fig S2(a) includes CSG2 nanocomposite, and the coated

CCTO NPs are well spread all over the GO sheet. High dielectric constant nature of CCTO NPs over GO enhances the dielectric values as compared to other CSG1 and CSG3 nanocomposites. But the same composite is remarkably showing a giant value of constant ε' and loss ε'' of 7.9×10^5 and 6.2×10^6 at 20 Hz. In comparison with CSG2, the other two composites, i.e. CSG1 and CSG3, show dielectric constant ε' of 9 and 53 with loss ε'' of 15 and -2 at the same frequency. Dielectric values are showing very low values that can be explained on the basis of surface area covered by the CCTO@SiO₂ core–shell NPs over GO NPs, which helps in a net polarization of dipoles or atoms present in both the materials in the presence of an applied electric field. When an electric field is applied to the material of CSG1 and CSG3, it is not capable of showing atomic polarization effectively, so it shows very low dielectric constant ε' as compared to CSG2, wherein CSG2 core–shell NPs help in the atomic polarization. Another reason attributed to the high dielectric constant and loss of CSG2, when the frequency reached up to 1×10^4 Hz, may be due to the dropping of dipole motion of dipole active atoms [37]. The dipoles present in the less decorated material, i.e. CSG1 and CSG3, are dropping with an increase in frequency; this is due to the less and more number of dipole active atoms. As the number of dipoles is less, the friction between dipoles against the surface of the precursor sheet will be less and contributes to the decrement of charge polarization attached to the material, helping in the increment of dielectric constant ε'. But in the case of CSG2, the number of dipoles is more, leading to less polarization of charges; hence, dielectric constant ε' decreases. The higher the dielectric loss ε'' of silica-coated CCTO–GO nanomaterial than the constant ε' (CSG2) can be used as in microwave technology. This phenomenon can be used for the application of microwave appliances [38]. CSG1 and CSG3 are showing a variable property which is not common in the dielectric study. But the explanation can be given as that the dielectric property shows a significant variation with the increase in

Figure 5 a Variation in dielectric constant (ε'), **b** dielectric loss (ε''), **c** impedance constant (Z') and **d** impedance loss (Z'') with respect to frequency of CSG1, CSG2 and CSG3 nanocomposites synthesized from 2–4-nm, 5–7-nm and 15–17-nm Si-coated CCTO, respectively.
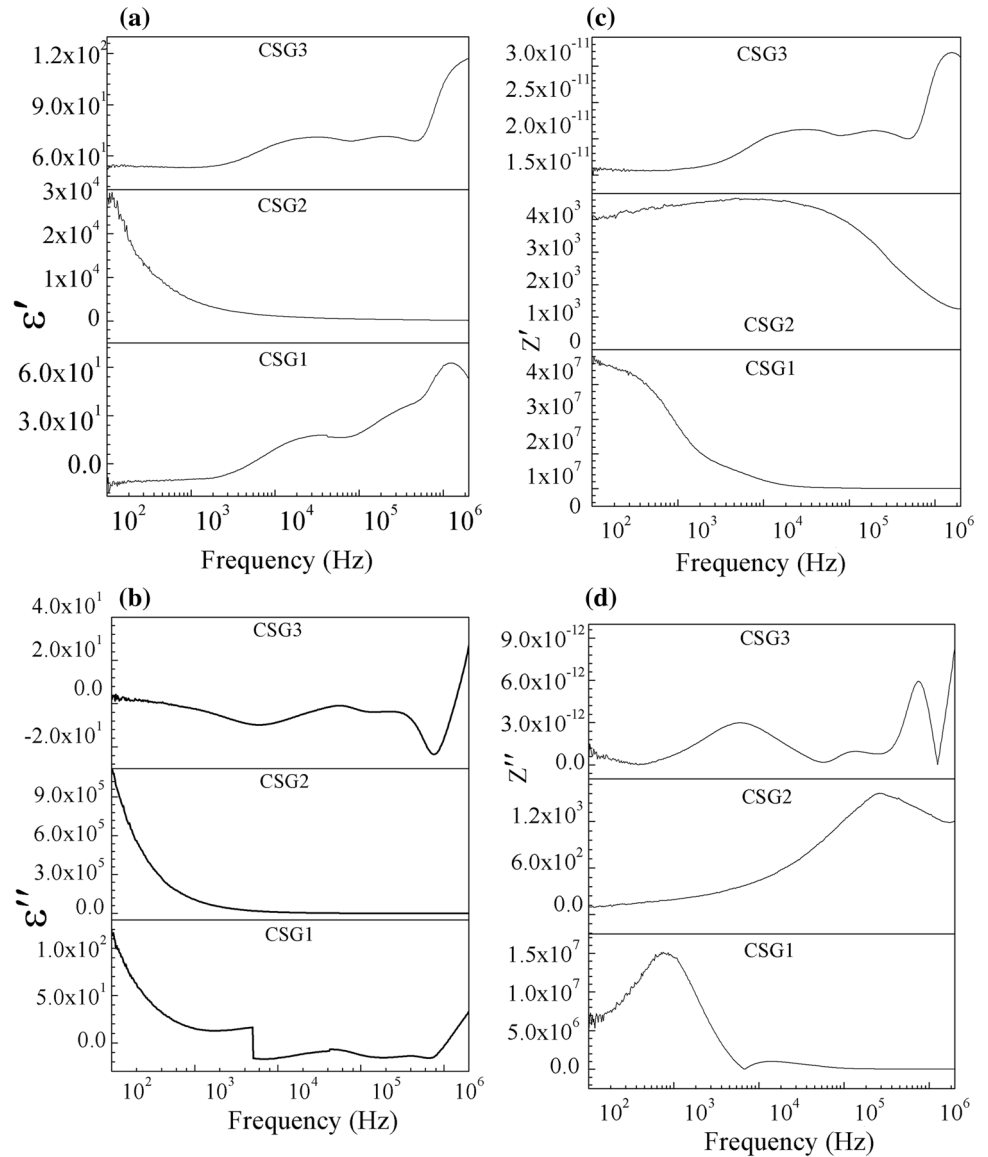
frequency at a constant room temperature; it may be due to the presence of dipoles like silica, ammine or CO_2 in the material that increases the friction which goes against dipole motion and helps in dropping of constant [22]. Another significant variation in this nanocomposite is may be due to the forces of attraction present in the material. We have already discussed a study about the presence of permanent dipoles inside the material, which may be affected by electronic polarization that leads to the electron shifting within the molecules. In a few cases, it is showing a negative dielectric constant and it may be due to the contribution of restoring force present in the isotropic sheet-like structure of GO NPs [39].

From the above discussion, it is clear that only CSG2 is showing the best result of dielectric constant as compared to other coated nanocomposites. Figure 5c, d confirms that CSG2 composite is giving lowest impedance value of $\sim 10^3$, whereas another composite is giving the value up to $\sim 10^7$. It confirms that CSG2 has a lower conductivity of electrons compared to other composites [40].

The temperature dependence of the dielectric study of silica-coated CCTO–GO nanocomposite

The temperature dependence of the dielectric study of silica-coated CCTO–GO composite shows a

variable observation. From earlier studies, it is clear that there can be a variation in dielectric constant with the increase in temperature and it may due to the crystallinity of the material or due to the atomic arrangement or may be due to some other physical behaviours like the presence of permanent dipoles like secondary amines. The presence of secondary amine groups in the material shows the presence of H bonding attached to the N atom, leading to the permanent dipole effect slightly less, but still, it behaves like a permanent dipole. (See scheme 1 for bonding interaction.) Earlier studies give the information that the presence of permanent dipole inside a material will contribute to the significant variation in dielectric constant ε' with temperature which can be explained in our study. The CSG2 material shows the best dielectric flow as we see in Fig. 6b. Figure 6b shows an explanatory image of temperature-dependent dielectric behaviour. It shows the decrease of ε' 7×10^2 to 3×10^2 with the temperature range from RT to 175 °C may be due to the loss of organic groups like hydroxyl or amine groups which have attended their respective boiling points and ceases the charge polarization. But after reaching 175 °C, ε' started to increase till it reaches up to a higher temperature and can be explained on the basis of structural disturbance occurs. The structural disturbance may occur due to the vanishing of hydroxyl/–COOH groups in GO to form various bonding interactions with the amine or silica group of core–shell CCTO@SiO$_2$ NPs and make it as defective structure. The formation of covalent C–N or van der Waals O–Si –H may also play a role in varying the dielectric constant. Figure 6a, c shows that the images of CSG1 and CSG3 have clearly given an idea that with an increase in shell thickness of silica-coated CCTO on GO sheet the dielectric constant is also increasing. Here CSG3 gives highest ε' of $\sim 1.3 \times 10^4$ (fig S4), while CSG1 and CSG2 are giving around 1×10^3 and 1×10^2. These two composites have shown an irregular dielectric behaviour as compared to CSG2. Figure 6a shows that at high temperature, ε' is slightly decreasing may be due to the polarity effect. The polar groups present in the materials like SiO$_2$ affect the disturbance to the alignment of dipoles like leftover substituted amine for which it causes a decrease of ε' at high temperature [41, 42]. Hence, CSG3 composite possessed a high dielectric constant up to 10^4 value is due to the more amount of silica present in the material (Fig S2(a)) and Fig S4 also confirmed that this composite is
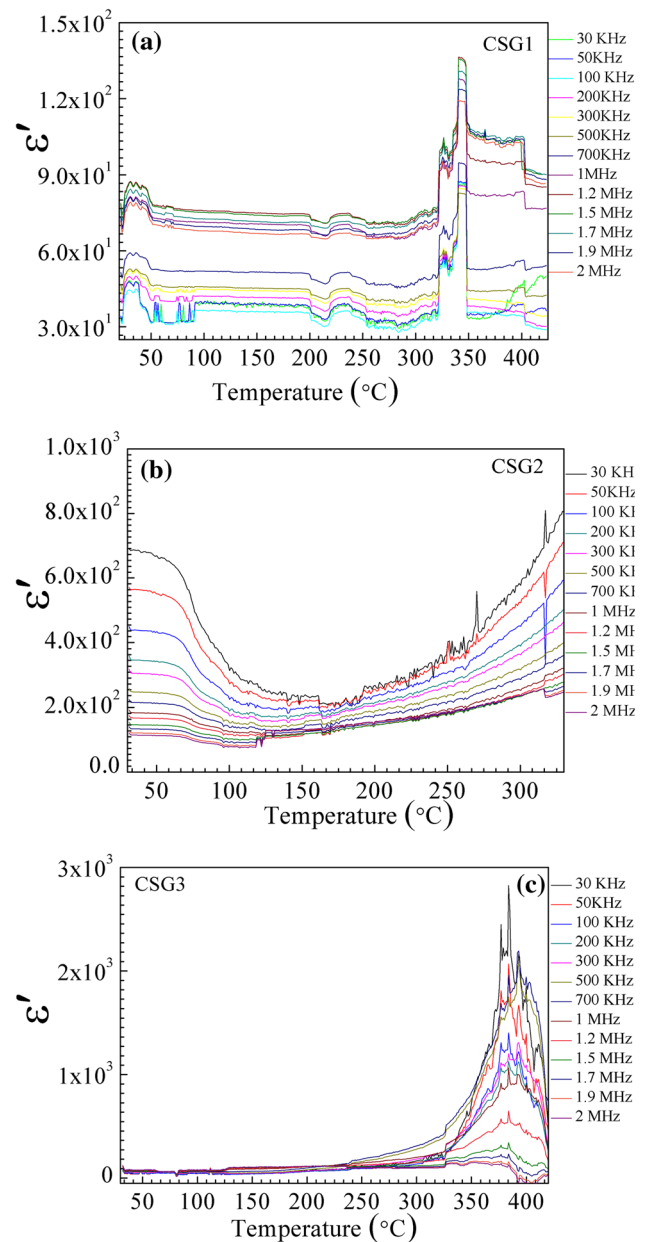

Figure 6 Variation in dielectric constant with different temperatures from RT to 400 °C at variable frequency region for of a CSG1, b CSG2 and c CSG3 nanocomposites synthesized from 2–4-nm, 5–7-nm and 15–17-nm Si-coated CCTO, respectively.

even stable up to 550 °C possessing constant up to $\varepsilon' \sim 1.15 \times 10^4 \sim 1.3 \times 10^4$ for 500 kHz and 700 kHz, respectively, with all other frequencies in a descending order.

Cole–Cole plot for nanocomposites

These three synthesized nanocomposites of GO–CCTO@SiO$_2$ are showing a very dissimilar type of Cole–Cole plot among themselves, ranging in low- and the high-frequency region. Figure 7a shows that CSG1 and c CSG3 represent two semicircle segments proving the presence of two type of dielectric
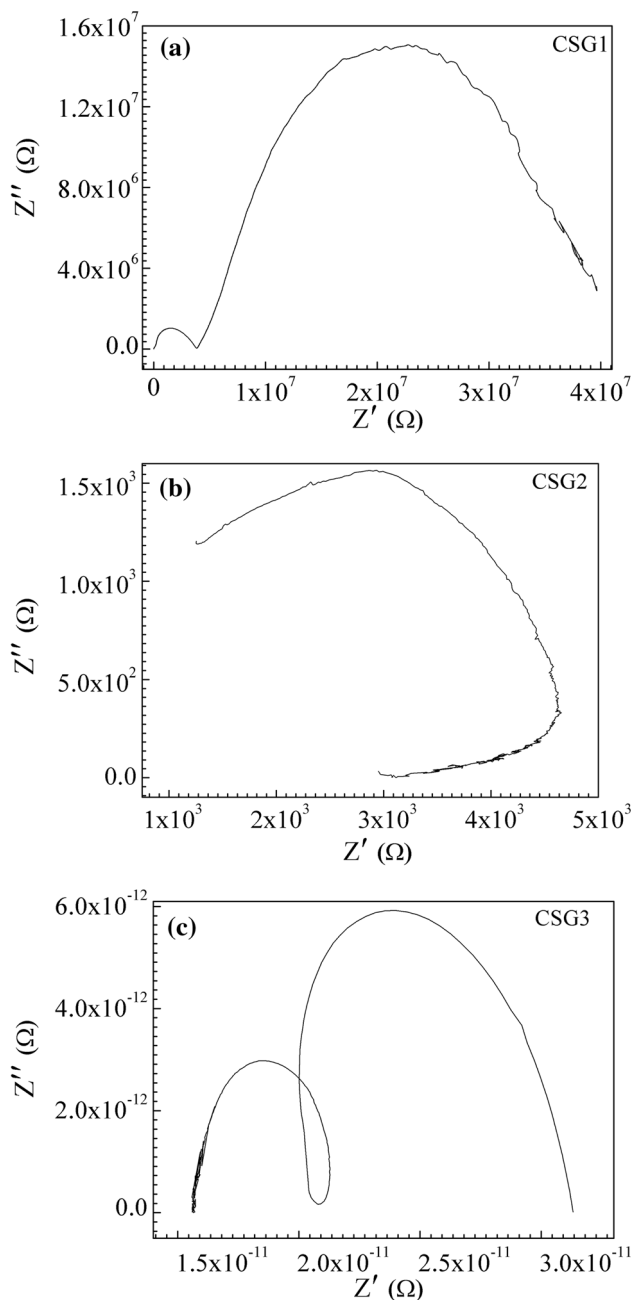
relaxation for decorated material as the dipoles present in them have relaxed twice [13]. This type of two semicircles are due to the interaction of basal plane and functional groups like epoxy (–O–), carboxyl (–COOH) or hydroxyl (–OH) groups present in GO with applied field or may be due to the interfacial polarization occurred due to the decoration between GO and core–shell NPs which is mentioned in our previous work [22]. CSG2 with the highest decoration has shown a distorted semicircle maybe due to the relaxation caused by loss of conductivity in CCTO NPs. In the case of CSG2, all dipoles have relaxed in a single phase of time wherein the cases of CSG1 and CSG3 have accomplished with two relaxation times, resulting in them to two semicircles. Hence, highest decorated material has shown a perfect Cole–Cole plot than other synthesized composites.

Conclusion

In this work, a series of CCTO@SiO$_2$–GO nanocomposites have been prepared through a novel synthesis method. Silica-coated CCTO NPs decoration over the surface of GO plays a vital role in the successful synthesis which mainly considers few environmental conditions like balanced atmospheric condition, stirring and centrifugation rpm, sonication time duration and amount of solute. It shows a variable study of dielectrics with respect to the different temperatures and frequencies. The material shows a high ε' of 1.5×10^4 after 500 °C which can be used as a good dielectric material for the electronic devices to be used as sensors, charge storage devices, etc. High loss was also observed more than constant at corresponding frequencies, leading to its use in the microwave electronic device industry. Concluding to this manuscript, the prepared nanocomposite can be used as a good dielectric material with the variation in the thickness of silica decoration over CCTO NPs and GO sheet. Even though many reports have given an idea about being used in the wide areas, our work has established new nanocomposites which can be used in designing new functional electronic devices and electrochemistry.

Figure 7 Cole–Cole plot in the low- and high-frequency region for of a CSG1, b CSG2 and c CSG3 nanocomposites, respectively.

Acknowledgements

Compliance with ethical standards

Conflict of interest The authors declare that they have no conflict of interest.

Electronic supplementary material: The online version of this article (https://doi.org/10.1007/s10853-019-03336-8) contains supplementary material, which is available to authorized users.

References

[1] Article P (2007) The rise of graphene. Nat Mater 6:183–191. https://doi.org/10.1038/nmat1849

[2] Kopelevich Y, Esquinazi P (2007) Graphene physics in graphite. Adv Mater 19:4559–4563. https://doi.org/10.1002/adma.200702051

[3] Bonaccorso F, Sun Z, Hasan T, Ferrari AC (2010) Graphene photonics and optoelectronics. Nat Photon 4:611–622. https://doi.org/10.1038/nphoton.2010.186

[4] Stankovich S, Dikin DA, Dommett GHB et al (2006) Graphene-based composite materials. Nature 442:282–286. https://doi.org/10.1038/nature04969

[5] Lee C, Wei X, Kysar JW, Hone J (2008) Measurement of the elastic properties and intrinsic strength of monolayer graphene. Science 321:385–388. https://doi.org/10.1126/science.1157996

[6] Zeng R, Luo Z, Zhang L, Tang D (2018) Platinum nanozyme-catalyzed gas generation for pressure-based bioassay using polyaniline nanowires-functionalized graphene oxide framework. Anal Chem 90:12299–12306. https://doi.org/10.1021/acs.analchem.8b03889

[7] Shu J, Qiu Z, Tang D (2018) Self-referenced smartphone imaging for visual screening of H_2S Using Cu_xO-polypyrrole conductive aerogel doped with graphene oxide framework. Anal Chem 90:9691–9694. https://doi.org/10.1021/acs.analchem.8b03011

[8] Cai G, Yu Z, Ren R, Tang D (2018) Exciton–plasmon interaction between AuNPs/graphene nanohybrids and CdS quantum dots/TiO_2 for photoelectrochemical aptasensing of prostate-specific antigen. ACS Sensors 3:632–639. https://doi.org/10.1021/acssensors.7b00899

[9] Bunch JS, Verbridge SS, Alden JS et al (2008) Impermeable atomic membranes from graphene sheets. Nano Lett 8:2458–2462. https://doi.org/10.1021/nl801457b

[10] Dreyer DR, Park S, Bielawski CW, Ruoff RS (2010) The chemistry of graphene oxide. Chem Soc Rev 39:228–240. https://doi.org/10.1039/b917103g

[11] Berger C, Song Z, Li X et al (2006) Electronic confinement and coherence in patterned epitaxial graphene. Science 312:1191–1196. https://doi.org/10.1126/science.1125925

[12] Chen H, Müller MB, Gilmore KJ et al (2008) Mechanically strong, electrically conductive, and biocompatible graphene paper. Adv Mater 20:3557–3561. https://doi.org/10.1002/adma.200800757

[13] Gupta TK, Singh BP, Singh VN et al (2014) MnO_2 decorated graphene nanoribbons with superior permittivity and excellent microwave shielding properties. J Mater Chem A 2:4256. https://doi.org/10.1039/c3ta14854h

[14] Subramanian MA, Li D, Duan N et al (2000) High dielectric constant in $ACu_3Ti_4O_{12}$ and $ACu_3Ti_3FeO_{12}$ phases. J Solid State Chem 151:323–325. https://doi.org/10.1006/jssc.2000.8703

[15] Ramirez AP, Subramanian MA, Gardel M et al (2000) Giant dielectric constant response in a copper-titanate. Solid State Commun 115:217–220. https://doi.org/10.1016/S0038-1098(00)00182-4

[16] Homes CC, Vogt T, Shapiro SM et al (2001) Optical response of high-dielectric-constant perovskite-related oxide. Science 293:673–676. https://doi.org/10.1126/science.1061655

[17] Li J, Sleight AW, Subramanian MA (2005) Evidence for internal resistive barriers in a crystal of the giant dielectric constant material: $CaCu_3Ti_4O_{12}$. Solid State Commun 135:260–262. https://doi.org/10.1016/j.ssc.2005.04.028

[18] Ahmadipour M, Ain MF, Ahmad ZA (2016) A Short review on copper calcium titanate (CCTO) electroceramic: synthesis, dielectric properties, film deposition, and sensing application. Nano-Micro Lett 8:291–311. https://doi.org/10.1007/s40820-016-0089-1

[19] Yu H, Zhang B, Bulin C et al (2016) High-efficient synthesis of graphene oxide based on improved hummers method. Sci Rep 6:1–7. https://doi.org/10.1038/srep36143

[20] Wang MH, Zhang B, Zhou F (2014) Preparation and characterization of silica-coated $CaCu_3Ti_4O_{12}$. J Electron Mater 43:2607–2613. https://doi.org/10.1007/s11664-014-3156-8

[21] Zhang WL, Choi HJ (2012) Silica-graphene oxide hybrid composite particles and their electroresponsive characteristics. Langmuir 28:7055–7062. https://doi.org/10.1021/la3009283

[22] Kumar KS, Pittala S, Sanyadanam S, Paik P (2015) A new single/few-layered graphene oxide with a high dielectric constant of 10 6: contribution of defects and functional groups. RSC Adv 5:14768–14779. https://doi.org/10.1039/C4RA10800K

[23] Kim SD, Zhang WL, Choi HJ et al (2014) Electrorheological activity generation by graphene oxide coating on low-dielectric silica particles. RSC Adv 4:62644–62650. https://doi.org/10.1039/c4ra13357a

[24] Bykkam S, Rao K (2013) Synthesis and characterization of graphene oxide and its antimicrobial activity against klebsiella and staphylococus. Int J Adv Biotechnol Res 4:142–146. https://doi.org/10.1016/j.apcata.2015.10.042

[25] Wilson NR, Wilson NR, Pandey PA et al (2009) Graphene oxide: structural analysis and application as a highly transparent support for electron microscopy. ACS Nano 3:2547–2556. https://doi.org/10.1021/nn900694t

[26] Pu X, Zhang H-B, Li X et al (2014) Thermally conductive and electrically insulating epoxy nanocomposites with silica-coated graphene. RSC Adv 4:15297–15303. https://doi.org/10.1039/C4RA00518J

[27] Bhawal P, Ganguly S, Chaki TK, Das NC (2016) Synthesis and characterization of graphene oxide filled ethylene methyl acrylate hybrid nanocomposites. RSC Adv 6:20781–20790. https://doi.org/10.1039/C5RA24914G

[28] Song J, Wang X, Chang C-T et al (2014) Preparation and characterization of graphene oxide. J Nanomater 2014:1–6. https://doi.org/10.1155/2014/276143

[29] Kudin KN, Ozbas B, Schniepp HC et al (2008) Raman spectra of graphite oxide and functionalized graphene sheets. Nano Lett 8:36–41. https://doi.org/10.1021/nl071822y

[30] Xu Y, Feng Y, Li X et al (2017) Direct formation of reduced graphene oxide and graphene quantum dot composites by using ascorbic acid as high-performance binder-free supercapacitor electrodes. Int J Electrochem Sci 12:8820–8831. https://doi.org/10.20964/2017.09.08

[31] Miroshnikov Y, Grinbom G, Gershinsky G et al (2014) Do we need covalent bonding of Si nanoparticles on graphene oxide for Li-ion batteries? Faraday Discuss 173:391–402. https://doi.org/10.1039/C4FD00089G

[32] Dimiev AM, Tour JM (2014) Mechanism of graphene oxide formation. ACS Nano 8:3060–3068. https://doi.org/10.1021/nn500606a

[33] Arthi G, Paulchamy B, Lignesh BD (2015) A simple approach to stepwise synthesis of graphene oxide nanomaterial. J Nanomed Nanotechnol 6:2–5. https://doi.org/10.4172/2157-7439.1000253

[34] Stankovich S, Dikin DA, Piner RD et al (2007) Synthesis of graphene-based nanosheets via chemical reduction of exfoliated graphite oxide. Carbon N Y 45:1558–1565. https://doi.org/10.1016/j.carbon.2007.02.034

[35] Kang JH, Kim T, Choi J et al (2016) Hidden second oxidation step of Hummers method. Chem Mater 28:756–764. https://doi.org/10.1021/acs.chemmater.5b03700

[36] Schwenzer B, Kaspar TC, Shin Y, Gotthold DW (2016) Spectroscopic study of graphene oxide membranes exposed to ultraviolet light. J Phys Chem C 120:12559–12567. https://doi.org/10.1021/acs.jpcc.6b03033

[37] Gavrilyachenko VG, Kabirov YV, Panchenko EM et al (2013) Specific features of the dielectric spectrum of $CaCu_3Ti_4O_{12}$ in the low-frequency range. Phys Solid State 55:1651–1654. https://doi.org/10.1134/S1063783413080131

[38] Jesurani S, Kanagesan S, Velmurugan R, Kalaivani T (2012) Phase formation and high dielectric constant of calcium copper titanate using sol–gel route. J Mater Sci: Mater Electron 23:668–674. https://doi.org/10.1007/s10854-011-0468-9

[39] He H, Klinowski J, Forster M, Lerf A (1998) A new structural model for graphite oxide. Chem Phys Lett 287:53–56. https://doi.org/10.1016/S0009-2614(98)00144-4

[40] Song S, Zhai Y, Zhang Y (2016) Bioinspired graphene oxide/polymer nanocomposite paper with high strength, toughness, and dielectric constant. ACS Appl Mater Interfaces 8:31264–31272. https://doi.org/10.1021/acsami.6b08606

[41] Wang D, Bao Y, Zha JW et al (2012) Improved dielectric properties of nanocomposites based on poly(vinylidene fluoride) and poly(vinyl alcohol)-functionalized graphene. ACS Appl Mater Interfaces 4:6273–6279. https://doi.org/10.1021/am3018652

[42] Havinga EE (1961) The temperature dependence of dielectric constants. J Phys Chem Solids Pergamon Press 18:253–255. https://doi.org/10.1016/0022-3697(61)90169-X